Mon. Not. R. Astron. Soc. **000**, 000–000 (0000) Printed 27 January 2015 (MN LATEX style file v2.2)

CMB distortion from circumgalactic gas

Priyanka Singh[1] ⋆, Biman B. Nath[1], Subhabrata Majumdar[2] & Joseph Silk[3,4]
[1] *Raman Research Institute, Sadashivanagar, Bangalore, India, 560080*
[2] *Tata Institute of Fundamental Research, Mumbai, India, 400005*
[3] *Institut d'Astrophysique, 75014Paris, France*
[4] *The John Hopkins University, Baltimore MD 20218, USA*

arXiv:1408.4896v2 [astro-ph.CO] 26 Jan 2015

27 January 2015

ABSTRACT

We study the Sunyaev-Zel'dovich (SZ) distortion of the cosmic microwave background radiation (CMBR) from extensive circumgalactic gas (CGM) in massive galactic halos. Recent observations have shown that galactic halos contain a large amount of X-ray emitting gas at the virial temperature, as well as a significant amount of warm OVI absorbing gas. We consider the SZ distortion from the hot gas in those galactic halos in which the gas cooling time is longer than the halo destruction time scale. We show that the SZ distortion signal from the hot gas in these galactic halos at redshifts $z \approx 1$–8 can be significant at small angular scales ($\ell \sim 10^4$), and dominate over the signal from galaxy clusters. The estimated SZ signal for most massive galaxies (halo mass $\geqslant 10^{12.5}$ $M_\odot$) is consistent with the marginal detection by *Planck* at these mass scales. We also consider the SZ effect from warm circumgalactic gas. The integrated Compton distortion from the warm OVI absorbing gas is estimated to be $y \sim 10^{-8}$, which could potentially be detected by experiments planned for the near future. Finally, we study the detectability of the SZ signal from circumgalactic gas in two types of surveys, a simple extension of the SPT survey and a more futuristic cosmic variance-limited survey. We find that these surveys can easily detect the kSZ signal from CGM. With the help of a Fisher Matrix analysis, we find that it will be possible for these surveys to constrain the gas fraction in CGM, after marginalizing over cosmological parameters, to $\leqslant 33\%$, in case of no redshift evolution of the gas fraction.

Key words: Galaxies: halos — evolution; cosmology: cosmic microwave background

1 INTRODUCTION

The standard scenario of galaxy formation predicts that baryonic gas falls into dark matter potentials and gets heated to the virial temperature (Silk 1977; White & Rees 1978; White & Frenk 1991). This gas then cools radiatively, and if the temperature is low enough ($T \leqslant 10^6$ K) for significant radiation loss, then most of the galactic halo gas drops to low temperature and no accretion shock develops in the halo (Birnboim & Dekel 2003). In the case of low mass galaxies, most of the accretion takes place through the infall of cold material from the intergalactic medium (IGM). However, in massive galaxies, the hot halo gas cools slowly and should remain warm/hot for a considerable period of time. This halo gas, if present, could potentially contain a large fraction of the baryons in the universe which is unaccounted for by collapsed gas and stars in galaxies, and could explain the missing baryon problem (Fukugita et al. 1998; Anderson & Bregman 2010).

Although numerical simulations have shown that disc galaxies should be embedded in a hot gaseous halo, this gas has been difficult to nail down observationally because of faintness of the X-ray emission (Benson et al. 2000; Rassmussen et al. 2009; Crain et al. 2010). Recent observations have finally discovered this hot coronal gas extended over a large region around massive spiral galaxies (Anderson & Bregman 2011; Dai et al. 2012; Anderson et al. 2013; Bogdán et al. 2013a,b; Anderson et al. 2014; Walker et al. 2014). The typical densities at galactocentric distances of $\geqslant 100$ kpc is inferred to be a few times 10^{-4} cm^{-3} (e.g., Bogdán et al. (2013b)), at a temperatures of ~ 0.5 keV. The amount of material implied in this extended region is unlikely to come from the star formation process, as shown by Bogdán et al. (2013a). An extended region of circumgalactic medium (CGM) has also been observed through OVI absorption lines around massive galaxies at $z \leqslant 1$ (Tumlinson et al. 2011), although these observations probe clouds at $T \sim 10^{5.5}$ K.

At the same time, the presence of hot halo gas around the Milky Way galaxy has been inferred via ram

⋆ priyankas@rri.res.in

pressure arguments from the motion of satellite galaxies (Grcevich & Putman 2009; Putman et al. 2012; Gatto et al. 2013). These observations suggest that the density profile of the hot coronal gas in our Galaxy is rather flat out to large radius, with $n \sim 10^{-3.5}$ cm^{-3}. Theoretically, one can understand this profile from simple modelling of hot, high entropy gas in hydrostatic equilibrium (Maller & Bullock 2004; Sharma et al. 2012; Fang et al. 2013). While in galaxy clusters, the high entropy of the diffuse gas produces a core, for massive galaxies (with implied potential wells shallower than in galaxy clusters), the core size is relatively large and extends to almost the virial radius.

One of the implications of this hot coronal gas in the halos of massive galaxies is the SZ distortion of the CMBR (Planck Collaboration XI 2013). The average y distortion of the CMBR from massive galaxies is likely to be small. However, the anisotropy power spectrum could have a substantial contribution from the hot gas in galactic halos. The SZ distortion from galaxy clusters have been computed with the observed density and temperature profiles of the X-ray emitting gas, or the combined pressure profile (e.g, Majumdar (2001); Komatsu & Seljak (2002); Efstathiou & Migliaccio (2012)). In the case of the galactic halos, because of the expected flat density profile, the resulting y-distortion could be larger than that of galaxy clusters for angular scales that correspond to the virial radii of massive galaxies, i.e., $\ell \sim 10^4$. These angular scales are being probed now and therefore the contribution to the SZ signal from galactic halos is important. In this paper, we calculate the angular power spectrum from both the thermal and kinetic SZ effects, if a fraction $f \sim 0.11$ of the total baryonic content of massive galaxies is in the form of hot or ionized halo gas.

Although such a fraction of gas has been estimated from the observations of NGC 1961 and NGC 6753 (Bogdán et al. 2013a), it remains uncertain whether it is a representative value, or whether it can be as low as 0.05. Recent studies of absorption from halo gas along the lines of sight to background quasars show that roughly half of the missing baryons is contained in the halo as warm (at $\sim 10^4$ and $\sim 10^{5.5}$ K) components. We also discuss the possible SZ signatures from this cool-warm gas in galactic halos.

2 SUNYAEV-ZEL'DOVICH DISTORTION FROM HOT GALACTIC HALO GAS

For simplicity, we assume that galactic halos contain a constant fraction of the total halo mass, independently of the galaxy mass. If we consider the total baryon fraction $\Omega_b/\Omega_m \sim 0.16$, and the fraction of the total mass that is likely to be in the disc, which is predicted to be ~ 0.05 (Mo et al. 1998; Moster et al. 2010; Leauthaud et al. 2010; Dutton et al. 2010), then one can assume a fraction $f_{\rm gas} = 0.11$ of the total halo mass to be spread throughout the halo. We also assume it to be uniform in density, with a temperature given by the virial temperature of the halo. The uncertainties in gas fraction and temperature are explored later in Section 5.1. The cosmological parameters needed for our calculatiosn are taken from the recent Planck results (Table 2 of Planck Collaboration XVI (2013)).

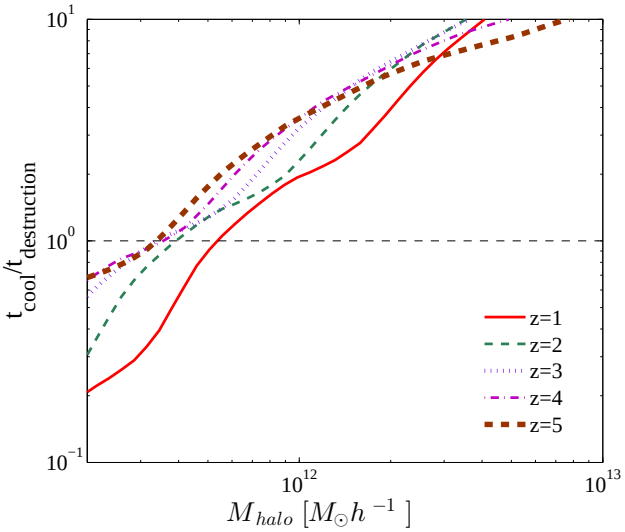

Figure 1. The ratio of cooling time to destruction time scale of halos is shown as a function of halo mass collapsing at $z = 1$ (red solid line), $z = 2$ (thin green dashed line), $z = 3$ (blue dotted line), $z = 4$ (magenta dot-dashed line) and $z = 5$ (thick brown dashed line).

2.1 Thermal Sunyaev-Zel'dovich effect

When CMBR photons are inverse Compton scattered by high energy electrons, the CMB spectrum is distorted giving rise to the thermal Sunyaev-Zel'dovich effect (tSZ). This effect is represented in terms of the Compton y-parameter defined as $y = (k_b T_e n_e \sigma_T L)/(m_e c^2)$ where σ_T is the Thomson scattering cross section, T_e is the temperature ($T_e >> T_\gamma$) and n_e is the electron density of the medium, considered to be uniform here, and ℓ is the distance traversed by the photons through the medium. The profile of y can be written in terms of the impact parameter w, or the angle $\theta = w/D_A$ (where D_A is the angular diameter distance) as

$$\begin{aligned} y(w) &= \frac{2 k_b T_v n_e \sigma_T}{m_e c^2} \sqrt{R_v^2 - w^2}\,, \\ y(\theta) &= \frac{2 k_b T_v n_e \sigma_T R_v}{m_e c^2} \sqrt{1 - \frac{D_A^2 \theta^2}{R_v^2}}. \end{aligned} \quad (1)$$

Here the electron density $n_e = \frac{\rho_{gas}}{\mu_e m_p}$ of the hot gas is determined by the requirement that the total hot gas mass within the virial radius is a fraction $f_g = 0.11$ of the halo mass. The virial radius of a halo of mass M collapsing at redshift z is given by

$$R_{vir} = 0.784 \Big(\frac{M}{10^8 h^{-1}}\Big)^{1/3} \Big(\frac{\Omega_M}{\Omega_M(z)} \frac{\triangle(z)}{18\pi^2}\Big)^{-1/3} \Big(\frac{1+z}{10}\Big)^{-1} h^{-1}\text{kpc} \quad (2)$$

where $\Omega_M(z) = \Omega_M (1+z)^3/E^2(z)$, the critical overdensity $\triangle(z) = 18\pi^2 + 82d - 39d^2$ and $d = \Omega_M(z) - 1$.
Later, we will also discuss the effect of varying f_g, including its possible redshift evolution. The temperature T_e corresponds to the virial temperature of the halo. We discuss in §3.2 below the appropriate mass and redshift range of galactic halos in which the gas likely remains hot.

2.2 Kinetic Sunyaev-Zel'dovich effect

If the scattering medium has bulk velocity with respect to the CMB frame, the CMBR is anisotropic in the rest frame of the scattering medium. The scattering makes the CMBR isotropic in the rest frame of the scattering medium, resulting in the distortion of the CMB spectrum with respect to the observer and giving rise to the kinetic Sunyaev-Zel'dovich effect (kSZ). The kSZ effect is proportional to the line of sight peculiar velocity and optical depth of the scattering medium. In the non-relativistic limit, the Compton y-parameter for the kSZ effect is defined as $y = (v_{\rm los} n_e \sigma_T L)/c$ where $v_{\rm los}$ is the line-of-sight peculiar velocity of the scattering medium. The tSZ effect and the kSZ effect have different frequency dependences which makes them easily separable with good multi-frequency data. In contrast to the tSZ effect, the spectral shape of the CMB is unchanged by the kSZ effect. In the Rayleigh-Jeans limit, the ratio of the change in CMB temperature caused by these two effects is :

$$\frac{\triangle T_{\rm kin}}{\triangle T_{\rm th}} \approx \frac{1}{2}\frac{v_{\rm los}}{c}\Big(\frac{k_b T_e}{m_e c^2}\Big)^{-1}, \approx 0.09\Big(\frac{v_{\rm los}}{1000\,{\rm km\,s^{-1}}}\Big)\Big(\frac{k_b T_e}{10\,{\rm kev}}\Big)^{-1} \quad (3)$$

For galaxy clusters, $k_b T_e \sim 10$ keV and $v_{\rm los} \sim$ few hundred km/sec which makes tSZ $\gg$ kSZ . But for the case of galaxies with virial temperature $T_e \sim 10^6$ K, hence $k_b T_e \sim 0.1$ keV, thus making kSZ > tSZ.

3 THE SZ POWER SPECTRUM

The SZ power spectrum arises by summing over the contributions from *all* the halos that would distort the CMB convolved with the template distortion for the halos as a function of mass and redshift; the distribution of the halos can be approximated by fits to outputs from N-body simulations. However, not all dark matter halos identified in the simulations would contribute to the SZ C_ℓ and one has to use *only* those galactic halos where the gas has not cooled substantially; this is discussed in detail in Section 3.2.

3.1 Thermal SZ C_ℓ

The thermal SZ template for contribution by a galactic halo is given by the angular Fourier transform of $y(\theta)$ (see Equation 1) and is given by

$$y_l \approx 2\pi\int_0^\pi \theta y(\theta) J_o[(l+1/2)\theta]d\theta\,, = \frac{4\pi k_b \sigma_T R_v}{m_e c^2}\int_0^\pi \theta T_v n_e \sqrt{1-\frac{D_A^2\theta^2}{R_v^2}}J_o\Big[(l+1/2)\theta\Big]d\theta = \frac{8 k_b T_v n_e \sigma_T R_v^{3/2}}{m_e c^2 D_A^{1/2}}(\frac{\pi}{2l+1})^{3/2}J_{3/2}\Big[(l+1/2)\frac{R_v}{D_A}\Big]\,. \quad (4)$$

The last equality follows from Gradshteyn & Ryzhik (1990).

The angular power spectrum due to the tSZ effect by hot diffuse gas in galactic halos is given by

$$C_l = g^2(x) C_l^{yy} \quad (5)$$

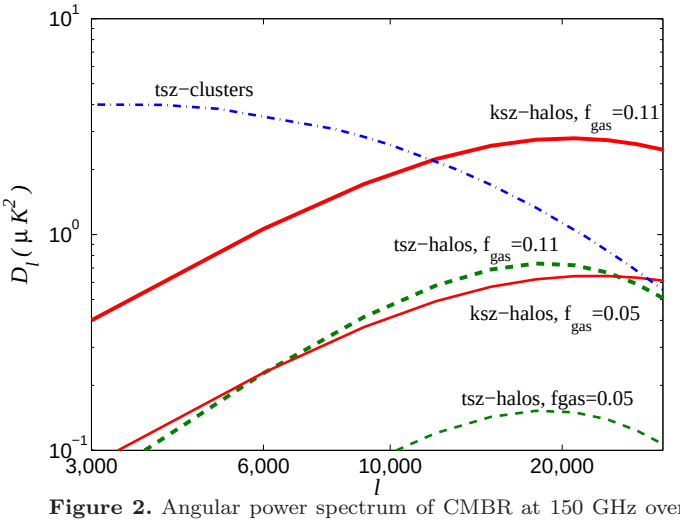

Figure 2. Angular power spectrum of CMBR at 150 GHz over a larger range of ℓ, for tSZ (green dashed line) and kSZ (red solid line) from galactic halos, compared with tSZ from clusters (blue dot-dashed line). Here the thick and thin lines correspond to $f_{gas} = 0.11$ and $f_{gas} = 0.05$ respectively.

Where $g(x) = x\coth(x/2) - 4$ and C_l^{yy} is frequency independent power spectrum.

$$C_l^{yy} = C_l^{yy(P)} + C_l^{yy(C)} \quad (6)$$

where $C_l^{yy(P)}$ is the Poisson term and $C_l^{yy(C)}$ is clustering or correlation term. These two terms can be written as (Komatsu & Kitayama 1999)

$$C_l^{yy(P)} = \int_0^{z_{\rm max}} dz \frac{dV}{dz}\int_{M_{min}}^{M_{\rm max}} dM \frac{dn(M,z)}{dM}|y_l(M,z)|^2$$
$$C_l^{yy(c)} = \int_0^{z_{\rm max}} dz \frac{dV}{dz} P_m(k=\frac{l}{r(z)},z) \times\Big[\int_{M_{min}}^{M_{\rm max}} dM \frac{dn(M,z)}{dM} b(M,z) y_l(M,z)\Big]^2\,. \quad (7)$$

Here $r(z) = (1+z)D_A$ is the comoving distance, $\frac{dV}{dz}$ is differential comoving volume per steradian, $P_m(k,z)$ is matter power spectrum, $b(M,z)$ is the linear bias factor, and $\frac{dn(M,z)}{dM}$ is the differential mass function. Here we have used the Sheth-Tormen mass function

$$\frac{dn}{dM}dM = A\sqrt{\frac{2\alpha\nu^2}{\pi}}\frac{\rho_m}{M^2}e^{-\alpha\nu^2}\Big[-\frac{d\log\sigma}{d\log M}\Big] \times\Big[1+\Big(\alpha\nu^2\Big)^{-p}\Big]dM\,, \quad (8)$$

where $A = 0.322184$, $\alpha = 0.707$ and $p = 0.3$ (Sheth & Tormen 2001). We have used the bias factor from Jing (1999),

$$b(M,z) = \Big(1+\frac{0.5}{\nu^4}\Big)^{(0.06-0.02n)}\Big(1+\frac{\nu^2-1}{\delta_c}\Big) \quad (9)$$

with $\nu = \frac{\delta_c}{D_g(z)\sigma(M)}$, where $D_g(z)$ is the growth factor, n is the index of primordial power spectrum , $\delta_c = 1.68$ is the critical overdensity and $\sigma(M)$ is the present day smoothed (with top hat filter) variance.

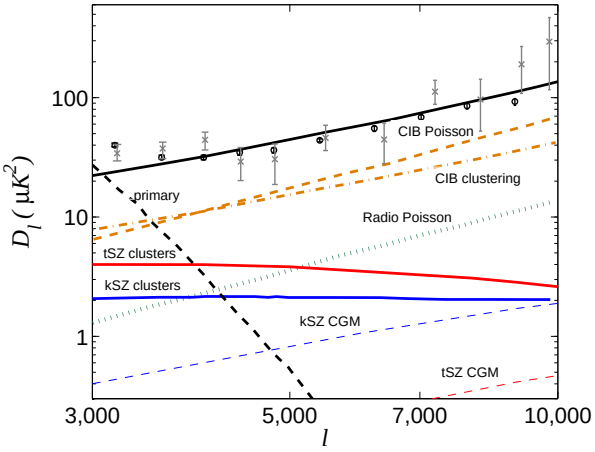

Figure 3. Angular power spectrum of CMBR at 150 GHz from different processes and compared with data points from ACT (grey bars) and SPT (black bars). The thermal SZ from galactic halos calculated here is shown in red (thick solid line), and the kSZ from galactic halos is shown in blue (thick solid line). Thermal SZ from galaxy clusters (Efstathiou & Migliaccio 2012) is shown in red (thin solid line) , the kinetic SZ from galaxy clusters is shown in blue (thin solid line), the radio poisson and CIB poisson signals in green dotted and brown dashed lines, respectively, and CIB clustering signal is shown in brown dot-dashed line. The lensed primary signal is shown in black and the total signal is shown by grey line.

3.2 Mass and redshift range

As mentioned earlier, not all the galactic halos given by the ST mass function (i.e Equation 8) will contribute to the SZ C_ℓ . For a realistic estimate of the CMB distortion from circum-galactic gas in galaxies, we need to use only those galactic halos in which the hot halo gas does not cool substantially, so that the hot gas persists for a considerable period of time and can contribute to the anisotropy. The cooling time of the gas is defined as $t_{\rm cool} = 1.5nkT/(n_e^2\Lambda(T))$, where n is the particle density ($\sim \frac{\mu_e}{\mu} n_e$), μ is mean molecular weight of the gas, ν_e is the mean molecular weight per free electron and $\Lambda(T)$ is the cooling function. We assume the galactic halo gas to be of metallicity 0.1 $Z_\odot$, and use the cooling function from (Sutherland & Dopita 1993).

This cooling time should be compared with a time scale corresponding to the destruction of these galactic halos in the merger or accretion processes, which would lead to the formation of larger halos. Every merging event leads to heating of the halo gas back to the virial temperature. It is therefore reasonable to assume that the halo gas would remain hot at the virial temperature if the cooling time is longer than the time corresponding to the destruction of halos.

We have used an excursion set approach to calculate the destruction time (Lacey & Cole 1993, 1994). For Press-Schechter mass function the destruction time for a galactic halo of mass M at time t is

$$t_{dest}(M,t) = [\phi(M,t)]^{-1}, \\ = \Big[\int_{M(1+\epsilon)}^{\infty} \tilde{Q}(M,M_1;t)dM_1\Big]^{-1} \quad (10)$$

Where $\tilde{Q}(M,M_1;t)$ is the probability that an object of mass M grows into an object of mass M_1 per unit time through merger or accretion at time t.

$$\tilde{Q}(M,M_1;t)dM_1 = \sqrt{\frac{2\sigma^2(M_1)}{\pi}}\Big[\frac{\sigma^2(M)}{\sigma^2(M_1)(\sigma^2(M)-\sigma^2(M_1))}\Big]^{\frac{3}{2}} \\ \times\Big|\frac{d\delta}{dt}\Big|\exp\Big[-\frac{\delta^2(\sigma^2(M)-\sigma^2(M_1))}{2\sigma^2(M)\sigma^2(M_1)}\Big] \\ \times\Big|\frac{d\sigma(M_1)}{dM_1}\Big|dM_1 \quad (11)$$

Here we have used $\epsilon = 0.1$. For the mass range considered, the destruction time for Sheth-Tormen mass function and Press-Schechter mass function give similar results (Mitra et al. (2011)). For simplicity we have used the Press-Schechter mass function to calculate the destruction time.

We show the ratio of the cooling time to destruction timescale as a function of mass at different redshifts in Figure 1. Based on this estimate, we use those galactic halos in our calculation of CMBR anisotropy for which $t_{\rm cool}/t_{\rm dest} \geqslant 1$, so that gas in these galactic halos cannot cool quickly. This condition is used to determine the lower mass limit of galactic halos M_{min} in Equation 7. We have used $M_{\rm max} = 10^{13}h^{-1}M_\odot$ for the upper mass limit. For upper redshift limit of integration in Equation 7 it is sufficient to take $z_{\rm max} = 8$ (see Figure 4).

3.3 Kinetic-SZ C_ℓ

Analogously to the tSZ effect, the angular Fourier transform of Compton y-parameter for the kSZ effect is given by:

$$y_l \approx 8\frac{v_{\rm los}}{c}\frac{n_e\sigma_T R_v^{3/2}}{D_A^{1/2}}\Big(\frac{\pi}{2l+1}\Big)^{3/2}J_{3/2}\Big[(l+1/2)\frac{R_v}{D_A}\Big]. \quad (12)$$

A crucial input into the calculation of the kinetic-SZ C_ℓ is the line of sight peculiar velocity the dark matter halo which depends on its mass M, redshift and the overdensity of the environment δ in which the halo is present (Sheth & Diaferio 2001; Hamana et al. 2003; Bhattacharya & Kosowsky 2008). The probability distribution function of the line of sight velocity of a halo with mass M located in a region of overdensity δ is

$$p(v_{\rm los}|M,\delta,a) = \sqrt{\frac{3}{2\pi}}\frac{1}{\sigma_v(M,a)}\exp\Big(-\frac{3}{2}\Big[\frac{v}{\sigma_v(M,a)}\Big]^2\Big) \quad (13)$$

with the 3D velocity dispersion given by

$$\sigma_v(M,a) = [1+\delta(R_{\rm local})]^{\mu(R_{\rm local})}\sigma_p(M,a), \\ = [1+\delta(R_{\rm local})]^{\mu(R_{\rm local})}aH(a)D_a\Big(\frac{d\ln D_a}{d\ln a}\Big) \\ \times\Big(1-\frac{\sigma_0^4(M)}{\sigma_{-1}^2(M)\sigma_1^2(M)}\Big)^{1/2}\sigma_{-1}(M), \quad (14)$$

where $\sigma_p(M,a)$ is the rms peculiar velocity at the peaks of the smoothed density field and σ_j's are the moments of initial mass distribution defined as

$$\sigma_j^2(M) = \frac{1}{2\pi^2}\int_0^\infty dk k^{(2+2j)}P(k)W^2(kR(M)). \quad (15)$$

Here the smoothing scale $R(M)$ is given by $\Big(\frac{3M}{4\pi\rho_m}\Big)^{1/3}$, $W(kR)$ is the top hat filter and ρ_m is the present day mean matter density. The dependence of peculiar velocity on its

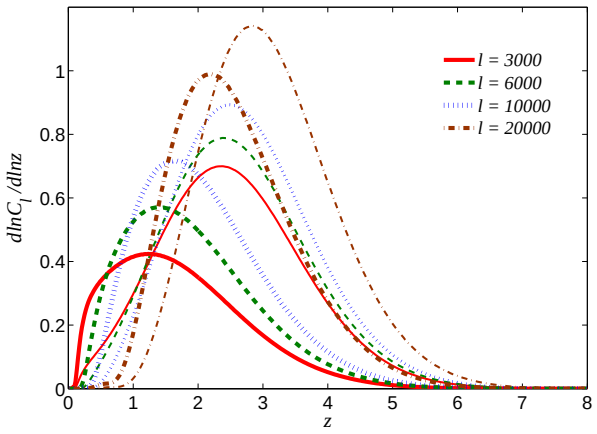

Figure 4. Redshift distribution of thermal and kinetic SZ effects. tSZ cases are shown with thin lines and kSZ cases, with thick lines for $l = 3000$ (red solid lines), $l = 6000$ (green dashed lines), $l = 10000$ (blue dotted lines) and $l = 20000$ (brown dot-dashed lines).

environment is contained in parameters $R_{\rm local}$, $\mu(R_{\rm local})$ and $\delta(R_{\rm local})$. These parameters are obtained by the conditions (Bhattacharya & Kosowsky 2008)

$$\mu(R_{\rm local}) = 0.6\frac{\sigma_0^2(R_{\rm local})}{\sigma_0^2(10\,{\rm Mpc/h})}\,. \qquad (16)$$

with $\sigma_0(R_{\rm local}) = 0.5/\sqrt{(1+z)}$ and $\delta(R_{\rm local}) = \sqrt{\sigma_0(R_{\rm local})}$.

The angular power spectrum due to kSZ effect by this hot diffuse gas is independent of frequency and is given by

$$C_l^{yy} = C_l^{yy(P)} + C_l^{yy(C)} \qquad (17)$$

Where $C_l^{yy(P)}$ and $C_l^{yy(C)}$ are Poisson and clustering terms given by Equation 7.

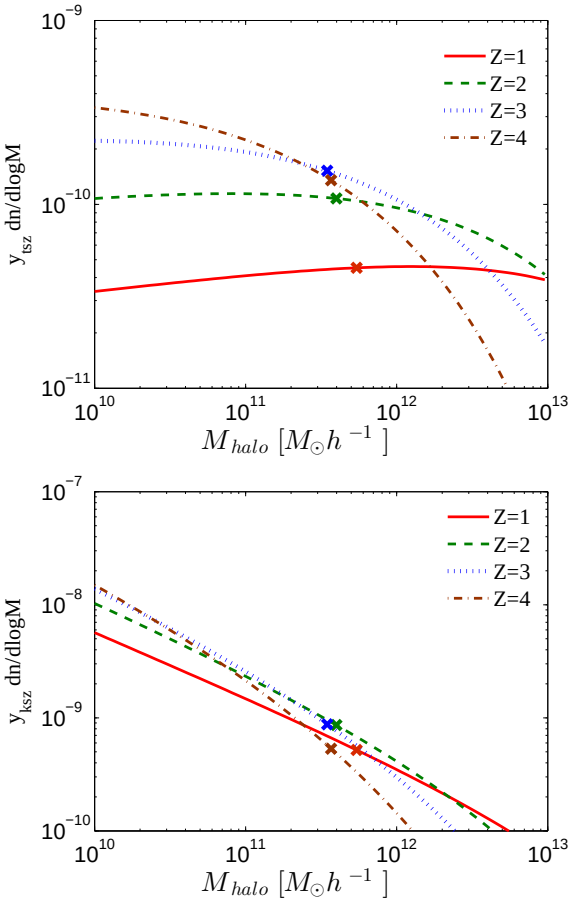

Figure 5. Moments of the mass function for tSZ (top panel) and kSZ (bottom panel), as a function of galactic halo masses, for redshifts $z = 1$ (red solid line), $z = 2$ (green dashed line), $z = 3$ (blue dotted line) and $z = 4$ (brown dot-dashed line). The cross markers on each line show the lower limits of masses considered in the calculations of SZ signal based on the cooling time scale being longer than halo destruction time scale.

3.4 SZ from CGM -vs- SZ from ICM

We plot the multipole dependence of both thermal and kinetic SZ C_ℓ from the CGM, in Figure 2, in term of the parameter $D_l = \frac{l(l+1)}{2\pi}C_l\overline{T^2}_{CMB}$ where $\overline{T}_{CMB}$ is present day mean CMB temperature in the units of μ K. In the same figure, we also plot the thermal SZ C_ℓ from hot gas in clusters of galaxies, the kinetic SZ C_ℓ from ICM being subdominant. We find that SZ C_ℓ 's from CGM peak above $\ell \sim 15000$, whereas the thermal SZ from ICM peaks at $\ell \sim 3000$ and then falls at higher ℓ-values.; the tSZ signal from CGM dominates that from ICM over $\ell > 13000$, whereas the kSZ from galactic halos overtakes tSZ from clusters earlier at $\ell > 10000$.

We have over-plotted South Pole Telescope (SPT) and Atacama Cosmology Telescope (ACT) data, with grey and black bars, respectively and auto correlation lines from Figure 4 of Addison et al. (2012) on top of SZ C_ℓ from galactic halos for a smaller range $3000 < \ell < 10000$ in Figure 3. The figure shows the contribution from thermal and kinetic SZ from galactic halos with red solid (thick) and blue solid (thick) lines. For comparison, the thermal and kinetic SZ signals from galaxy clusters are shown as red and blue solid (thin) lines. Also, the contribution from the sources responsible for the Cosmic Infrared Background (CIB) are shown, for both poisson (brown dashed line) and the clustered case (brown dot-dashed line). The contribution from clustering of radio sources is shown in green as a dotted line. The lensed primary signal is shown as a black dashed line. The comparison of tSZ and kSZ signals from galactic halos and galaxy clusters show that kSZ signal from galactic halos become comparable to galaxy cluster signals at $\ell \sim 10000$. This is because of the fact that kSZ is more important for lower mass halos, which correspond to smaller angles and larger ℓ values.

3.5 Redshift distribution of the angular power spectrum

The redshift distribution of C_l can be determined using

$$\frac{d\ln C_l}{d\ln z} = \frac{z\frac{dV}{dz}\int dM\frac{dn(M,z)}{dM}|y_l(M,z)|^2}{\int dz\frac{dV}{dz}\int dM\frac{dn(M,z)}{dM}|y_l(M,z)|^2} \qquad (18)$$

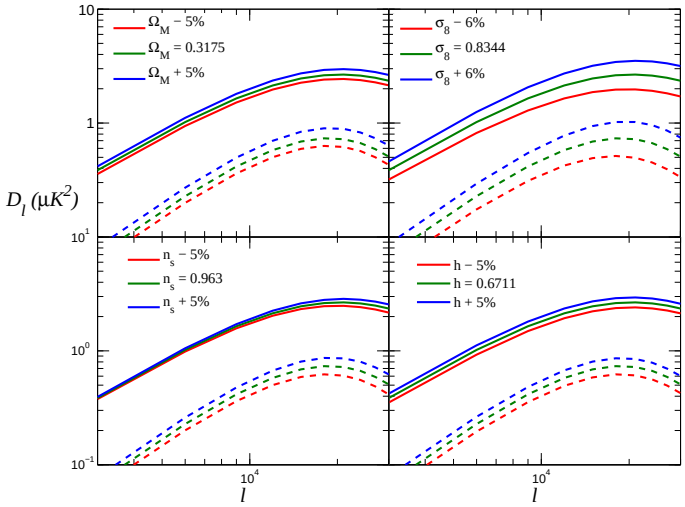

Figure 6. Dependence of SZ angular power spectrum on σ_8, Ω_M, n_s and h. Here the dashed lines are tSZ effect and the solid lines represent kSZ effect.

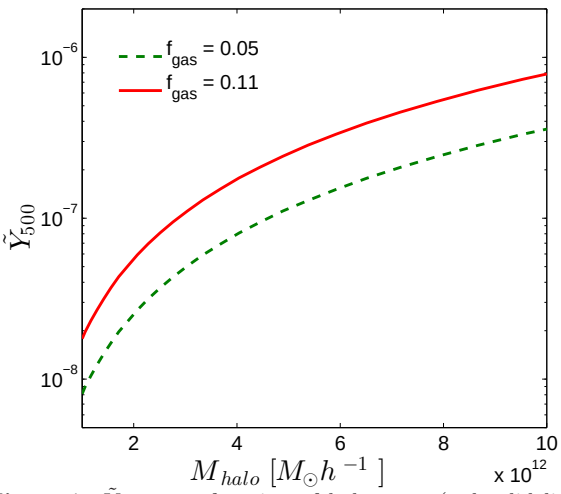

Figure 7. $\tilde{Y}_{500}$ as a function of halo mass (red solid line) for $f_{gas} = 0.11$ and $f_{gas} = 0.05$ (green dashed line).

We show the redshift distribution of C_l for $\ell = 3000, 6000, 10000$ and 20000 for tSZ and kSZ effect in Figure 4. For tSZ effect (shown in thin lines), for $\ell = 3000$, C_l has a peak at $z \sim 2$. This peak shifts to higher redshifts with increasing value of ℓ. For all ℓ values ($\ell > 3000$) there is non-negligible contribution to C_l coming from $z > 5$.

In case of the kSZ effect (thick lines), for $\ell = 3000$ there is a broad peak around $z \sim 1$–2 and the contribution to C_l is significant even below $z = 1$. The peak shifts to higher redshifts with increasing value of ℓ. The contribution from higher redshift becomes more important for larger ℓ values. Note that C_l scales as the square of the fraction of hot gas in galactic halos, and the plotted values assume the fraction to be 0.11. If the fraction is smaller, the values of C_l for kSZ and tSZ are correspondingly lower. For example, if the hot halo gas constitutes only half of the missing baryons, with a fraction ~ 0.05 (instead of 0.1), then SZ signal from galactic halos would dominate at $\ell \geqslant 30000$ (instead of 10^4).

3.6 Mass distribution

We can estimate the range of masses which contribute most to the thermal and kinetic SZ effects, by computing appropriate moments of the mass function, for pressure and peculiar velocity. Figure 5 shows the moment of $y-$parameters for tSZ and kSZ in the top and bottom panels, respectively, for the mass range 10^{10}–$10^{13} h^{-1} M_\odot$, corresponding to the l-range $\sim 7 \times 10^4$–7×10^3 for $z = 1$, and l-range $\sim 1.4 \times 10^5$–1.4×10^4 for $z = 4$. The moments of tSZ ($y_{\rm tSZ} \times \frac{dN}{d \log M}$) show that the dominant mass range decreases with increasing redshift, from being $\sim 10^{13}\ h^{-1}\ {\rm M}_\odot$ at $z \sim 1$, to halos of $\sim 5 \times 10^{11}\ h^{-1}\ {\rm M}_\odot$ at $z \sim 2$–3 to lower masses at higher redshift. From the redshift distribution information in Figure 4, we can infer that galactic halos with mass $\sim 10^{12}\ h^{-1}\ {\rm M}_\odot$ are the dominant contributors for $\ell \leqslant 10^4$ for tSZ effect.

The moments of the kSZ signal ($y_{\rm kSZ} \times \frac{dN}{d \log M}$) show that low mass galactic halos are the major contributors to the signal, and become progressively more important at increasing redshifts. Since we have constrained the mass range from a cooling time-scale argument, the moments at different redshift show that the dominant mass is $\sim 5 \times 10^{11}\ h^{-1}$ $\rm M_\odot$ for $z \sim 1$–3. Again, from the redshift distribution information in Figure 4, this implies that galactic halos with $\sim 10^{12}\ h^{-1}\ {\rm M}_\odot$ are the major contributors, as in the case of tSZ effect. Since significant contribution for tSZ and kSZ comes from low mass halos, our predictions are sensitive to the assumed lower mass in which the hot halo gas can remain hot until the next merging event.

3.7 Dependence of SZ angular power spectrum on cosmological parameters

We also calculate the dependence of the SZ angular power spectrum on different cosmological parameters. In Figure 6, we plot the dependences of tSZ and kSZ signals on σ_8, Ω_M, n_s and h with dashed and solid lines, respectively. When one cosmological parameter is varied, others are kept fixex. However, when Ω_M is varied, Ω_Λ is also changed to keep $\Omega_M + \Omega_\Lambda = 1$.

The dependences of C_l on different cosmological parameters can be fit by power-law relations near the fiducial values of the corresponding parameters. For example, we find that near the fiducial value of σ_8, $C_l \propto {\sigma_8}^6$, which is similar to the dependence of tSZ signal from galaxy clusters (Komatsu & Seljak 2002). For other parameters, we have, for tSZ, $C_l \propto {\Omega_M}^3$, $C_l \propto {n_s}^{7/2}$ and $C_l \propto h^3$ for tSZ. The corresponding dependences for kSZ are: $C_l \propto {\sigma_8}^5$, $C_l \propto {\Omega_M}^2$, $C_l \propto n_s$ and $C_l \propto h^2$.

4 DETECTABILITY IN FUTURE SURVEYS AND CONSTRAINING GAS PHYSICS

4.1 Integrated Comptonization parameter $\tilde{Y}_{500}$

Next we estimate the integrated Comptonization parameter for CGM. The Comptonization parameter Y_{500} (due to tSZ)

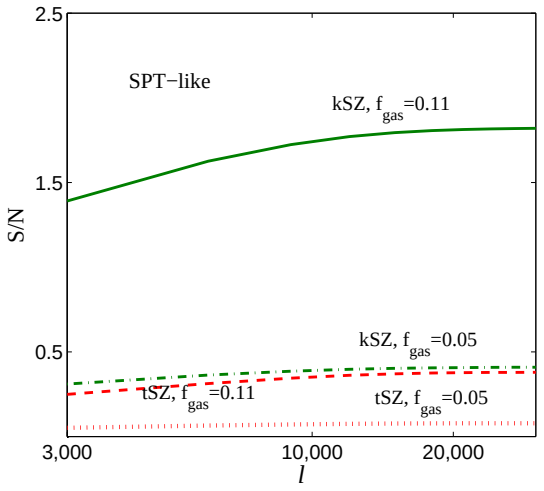

Figure 8. The cumulative signal to noise ratio (SNR) as a function of ℓ_{max}, in case of SPT-like survey, with $\ell_{min} = 3000$. The upper line corresponds to kSZ and the lower line to tSZ. The solid (green) and dashed (red) lines corresponds to kSZ and tSZ for $f_{\rm gas} = 0.11$, respectively, and the dot-dashed (green) and dotted (red) lines, for $f_{\rm gas} = 0.05$.

Table 1. Fiducial values and priors on the parameters

Parameter	Fiducial value	Prior-1	Prior-2	Prior-3
σ_8	0.8344	0.027	0.027	0.027
Ω_M	0.3175	0.020	0.020	0.020
n_s	0.963	0.0094	0.0094	0.0094
h	0.6711	0.014	0.014	0.014
$f_{\rm tratio}$	1.0	-	1.0	1.0
$f_{\rm Temp}$	1.0	-	-	0.25
$f_{\rm gas}$	0.11	-	-	-
$\alpha_{\rm gas}$	0.0	-	-	-

integrated over a sphere of radius R_{500} is

$$Y_{500} = \frac{\sigma_T}{m_e c^2}\int_0^{R_{500}} \frac{PdV}{D_A^2(z)} = \frac{\sigma_T n_e k_b T_e}{m_e c^2 D_A^2(z)}\frac{4\pi R_{500}^3}{3} \quad (19)$$

where $D_A^2(z)$ is the angular diameter distance, $P = n_e k_b T_e$ is pressure of electron gas and R_{500} is defined as the radius within which the mean mass density is 500 times the critical density of the universe. The second equality in the above equation is for the case of constant electron density and temperature. The integrated Comptonization parameter scaled to z=0 is defined as

$$\tilde{Y}_{500} \equiv Y_{500} E^{-2/3}(z)\Big(\frac{D_A(z)}{500 Mpc}\Big)^2 . \quad (20)$$

Here $\tilde{Y}_{500}$ and Y_{500} are expressed in square arcmin.We show in Figure 7 the values of $\tilde{Y}_{500}$ as a function of halo mass for gas fractions $f_{0.11}$ and $f_{gas} = 0.05$. We have used the fit for concentration parameter (c) as a function of halo mass from Duffy et al. (2008).

From Table 1 of Planck Collaboration XI (2013), the lowest stellar mass bin for which SZ signal has been detected ($\tilde{Y}_{500} \sim 10^{-6}\,{\rm arcmin}^2$) is $M_* \sim 4 \times 10^{12} M_\odot$. This stellar mass corresponds to a virial mass $\sim 4.25 \times 10^{12} M_\odot h^{-1}$. From our calculations for a galactic halo of $M_{vir} \sim 4.25 \times 10^{12} M_\odot h^{-1}$ with $f_{gas} = 0.11$, the $\tilde{Y}_{500} \sim 0.2$–$0.3 \times 10^{-6}\,{\rm arcmin}^2$, consistent with the observed values (Table 1 of Planck Collaboration XI (2013)). If we use $f_{gas} = 0.05$, $\tilde{Y}_{500}$ goes down by roughly a factor of 2.

4.2 Signal to noise ratio in future surveys

The detectability of the CMB distortion from circumgalactic baryons can be estimated by calculating the cumulative Signal-to-Noise-Ratio (SNR) of the SZ power spectrum for a particular survey. For our purpose, we focus on two types of surveys, one which is an extension of the ongoing SPT survey to higher multipoles (although we show that the SNR from $\ell > 15000$ does not add much to the cumulative SNR), and a more futuristic survey which covers 1000 square degrees of the sky (i.e, $f_{\rm sky} \sim 2\%$) and is cosmic variance error limited. These are labeled 'SPT-like' and 'CV1000 ', respectively, for the rest of the paper:
(1) SPT-like survey: In this case we use $\ell_{\rm min} = 3000$ and $\ell_{\rm max} = 30000$. The noise in the measurement of C_l's (i.e. $\triangle C_l$) is taken from actual SPT data (Figure 4 of Addison et al. (2012)). These errors are then fitted with a power-law dependence on ℓ and extrapolated till $\ell = 30000$.
(2) CV1000 survey: This survey has 2% sky coverage and the error on C_l's are cosmic variance limited. Here, we have used a smaller ℓ-range and have taken $\ell_{\rm min} = 6000$ and $\ell_{\rm max} = 9000$.

The cumulative SNR, for SZ C_ℓ between $\ell_{\rm min}$ and $\ell_{\rm max}$, is given by

$${\rm SNR}_{\rm cumu}(\ell_{\rm min} < \ell_{\rm max}) = \Big(\Sigma_{\ell_{\rm min}\ell'_{\rm min}}^{\ell_{\rm max}} {\rm C}_\ell^{\rm X}({\rm M}_{\ell\ell'}^{\rm X})^{-1}{\rm C}_{\ell'}^{\rm X}\Big)^{1/2} \quad (21)$$

where X denotes cases tSZ, kSZ or Total, i.e tSZ+kSZ and $M_{\ell\ell'}^X$ is the corresponding covariance matrix, for any particular survey, given by

$$M_{\ell\ell'}^X = \frac{1}{4\pi f_{\rm sky}}\left(\frac{4\pi(C_\ell^X + N_\ell)^2}{(\ell+1/2)\triangle\ell}\delta_{\ell\ell'} + T_{\ell\ell'}^X\right) , \quad (22)$$

where N_ℓ is the noise power spectrum (after foreground removal) and $T_{\ell\ell'}^X$ is the SZ angular tri-spectrum (see, e.g., Komatsu & Kitayama (1999)). Note that this formula for the covariance matrix neglects the 'halo sample variance'.

The cumulative SNR provides a simple way to assess the constraining power of a given experiment irrespective of the constraints on particular parameters. We compute the cumulative SNR's for our two surveys, SPT-like and CV1000 surveys. Figure 8 shows the SNR as a function of $\ell_{\rm max}$ for the SPT-like survey. Note that the covariance matrix in Equation 21, in principle, should include all contributions from cosmic variance (Gaussian and non-Gaussian), experimental noise after foreground removal, as well as the tri-spectrum which represents the sample variance contribution to the covariance. However, for the halo masses of interest and the ℓ range of the contribution of the SZ discussed in this paper, the tri-spectrum can be neglected and the covariance matrices are, effectively, diagonal. For the CV1000 survey, the diagonal covariance matrix only contains the cosmic variance errors. The covariance matrix, for the SPT-like survey, is taken to be the noise (actual error bar) reported by the SPT and extrapolated to higher ℓ's (as explained earlier). In general, our extrapolation of SPT errors to higher ℓ-values

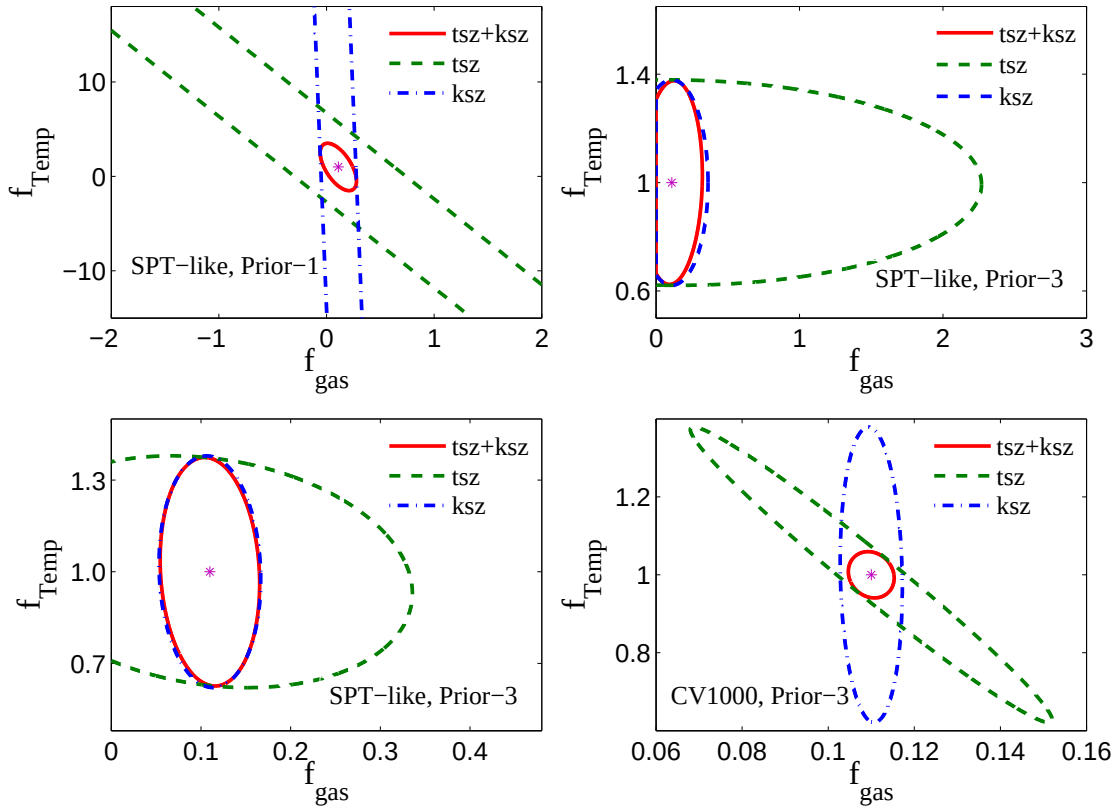

Figure 9. The figure shows the breaking of parameter degeneracy when information from tSZ C_ℓ and kSZ C_ℓ are taken together for different cases. The Upper Left panel shows result from the case Prior-1 , i.e., cosmological priors only, for the SPT-like survey even when α is fixed. The Upper Right panel shows the case Prior-3 which includes additional priors on $f_{\rm ratio}$ and $f_{\rm Temp}$ but α, now, varied for SPT-like . The Lower Left panel shows the case Prior-3 but with α fixed. The Lower Right panel shows the case for CV1000 for, with Prior-3 and α varied. In all cases, green dashed line is tSZ, blue dot-dashed is kSZ and solid red line is tSZ+kSZ.

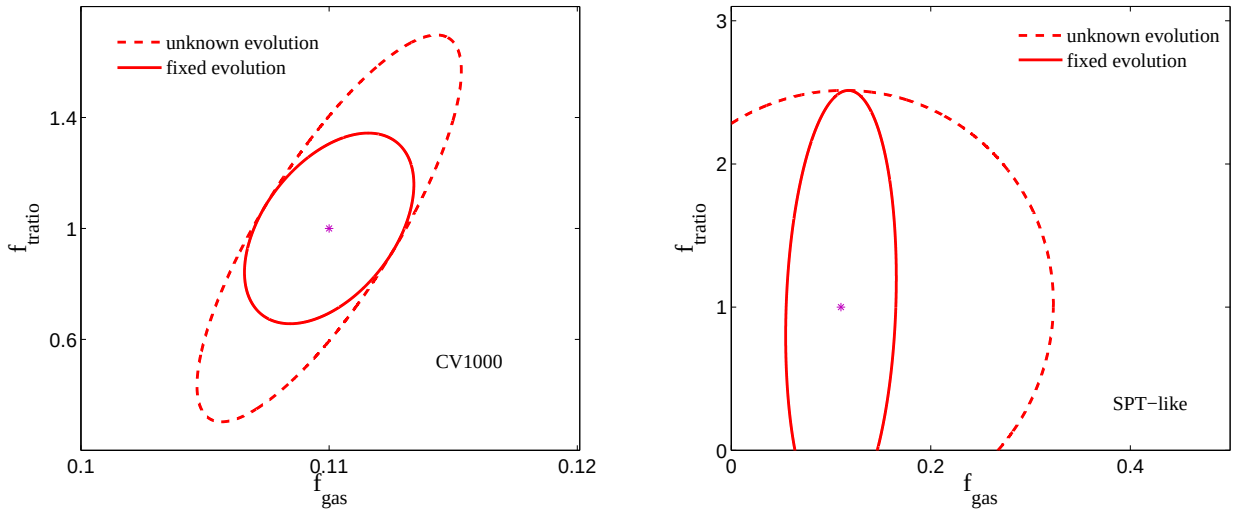

Figure 10. The figure shows the impact on parameter constraints due to any unknown evolution of the gas fraction with redshift parametrised as $f_{\rm gas}(z) = f_{\rm gas}[E(z)]^{\alpha_{\rm gas}}$. The Left Panel is for the survey 'CV1000 ' and Right Panel is for the survey 'SPT-like'. In both cases, the red dashed line corresponds to the case of $\alpha_{\rm gas}$ is unknown and varied as one of the Fisher parameters, whereas the red solid line correspond to $\alpha_{\rm gas}$ fixed at its fiducial value.

are conservative in nature as seen in Figure 8 - due to the increasing observational errors for higher multipoles, the SNR for the SPT-like survey flattens off beyond $\ell_{max} \sim 15000$. It is also evident from the figure, that although it would need a stringent handle on astrophysical systematics and better modelling of SZ C_ℓ from galaxy clusters to separate out the tSZ C_ℓ from CGM, kSZ signal from CGM has a signal to noise ratio $\sim 2\sigma$ for the SPT-like survey. If we take $l_{min} = 10000$ for SPT-like survey, the signal to noise ratio goes down roughly by a factor of 2 . In comparison, for the more futuristc CV1000 survey, the tSZ and the kSZ signal can be detected with a SNR of $\sim 600(950)$, at (upto) $\ell_{max} \sim 6000(9000)$.

5 FORECASTING

5.1 Formalism

We now employ the Fisher matrix formalism to forecast the expected constraints on the following parameters, focussing specially on the parameters related to gas physics of the circum-galactic baryons. The Fisher parameters considered are

$$\{[\sigma_8, \Omega_M, n_s, h], [f_{\rm gas}, f_{\rm tratio}, f_{\rm Temp}, \alpha_{\rm gas}]\} \ , \qquad (23)$$

where the first set within the parenthesis are the cosmological parameters and the second set, which depends on baryonic physics, are the *astrophysical* parameters.

To construct the Fisher Matrices for the two surveys, we compute the derivatives of the tSZ, kSZ and, hence, total SZ C_ℓ with respect to each parameter around the fiducial values listed in Table 1. Here $f_{\rm gas}$ is the redshift independent fraction of halo mass in gaseous form and $\alpha_{\rm gas}$ captures any possible evolution of the gas defined through $f_{\rm gas}(z) = f_{\rm gas}[E(z)]^{\alpha_{\rm gas}}$. Our fiducial model assumes no evolution of the gas fraction; see details in section 5.2.1. The other two parameters that encapsulate the uncertainty in our knowledge of hot gas in galactic halos are $f_{\rm tratio} = \frac{t_{\rm cool}}{t_{\rm dest}}$, i.e., the ratio of cooling time to destruction time for galactic halos, $f_{\rm Temp} = \frac{T}{T_{\rm vir}}$, i.e., the ratio of the temperature of the gas to the virial temperature of gas in a halo.

For a given fiducial model, the Fisher matrix is written as

$$F_{ij} \ = \ \frac{\partial C_\ell^X}{\partial p_i} (M_{\ell\ell'}^X)^{-1} \frac{\partial C_{\ell'}^X}{\partial p_j} \qquad (24)$$

where $M_{ll'}$ is given by equation 22 in case of CV1000 survey and for SPT-like survey we have $M_{ll} = (\Delta C_\ell^{SPT})^2$. Here ΔC_ℓ^{SPT}'s are the error on C_ℓ's from SPT data. The fiducial values and the priors used are listed in Table 1. Note that in all our calculations, cosmological priors are always applied. Priors related to gas/halo physics are additionally applied, on a case by case basis. For the rest of the paper, we denote the different priors uses as follows:

Prior-1 : Priors on cosmological parameters only.

Prior-2 : Priors on cosmological parameters + 100% prior on $f_{\rm tratio}$.

Prior-3 : Priors on cosmological parameters + 100% prior on $f_{\rm tratio}$ + 25% prior on $f_{\rm Temp}$.

In Prior-3 and Prior-2 , we have assumed a 100% prior on $f_{\rm tratio}$, reflecting the maximum uncertainty in this parameter. For $f_{\rm Temp}$, we have assumed a smaller uncertainty, since our constraint that cooling time is longer than the destruction time ensures that the gas temperature to be close to the virial temperature.

Additionally, for each case considered, we look at constraints for all the 8 parameters listed above (equation 23) and in the second case, we repeat the same procedure but with only 7 parameters, assuming that the baryonic content of galaxies is independent of redshift (i.e. $\alpha_{\rm gas} = 0$). The introduction of varying gas fraction in halos changes the shape of C_ℓ (see, for example, in Majumdar (2001))which results in different sensitivity to the Fisher parameters; it also introduces an extra nuisance parameter to be marginalised over. The results of the first analysis (with $\alpha_{\rm gas}$ varying) are shown in Table 3 and the second case (with $\alpha_{\rm gas}$ fixed) in Table 2.

5.2 Results

We are in an era in cosmology where major surveys like *Planck* have already provided tight constraints on the parameters of the standard cosmological model. In the future, two of the major goals are to go beyond the standard model of cosmology and to constrain parameters related to baryonic/gas physics associated with non-linear structures. One of the puzzles related to baryonic matter is the issue of 'missing baryons', i.e the fact that after accounting for the gas locked up in structures (like galaxies and galaxy clusters) and the diffuse intergalactic medium, one still falls short of the cosmological mean baryon fraction Ω_B. While recently, much of this missing material may have been accounted by the intra-cluster medium, a deficit of the order of at least ~ 10's % is still found.

With the growing observational evidence for CGM, it would be interesting to determine if its inclusion in the baryon census can fill the deficit. To go forward, one needs to go beyond the discovery of the CGM in nearby isolated halos (other than the Milky Way) or beyond what one can measure by doing a stacking analysis of gas in a sample of halos. This is possible by probing the locked gas in and around a cosmological distribution of galaxy halos through its signature on the CMB as shown in this paper. A constraint on the mean gas fraction, $f_{\rm gas}$, included in our calculations, provides one of the best ways to estimate the amount of circum-galactic baryons in a statistical sense. In the rest of the section, we focus on the constraints on $f_{\rm gas}$, for a variety of survey scenarios.

The constraints on the amount of baryons locked up as CGM, as well on other Fisher parameters, are shown in Tables 2 & 3. The 1σ ellipses for joint constraints of $f_{\rm gas}$ with non-cosmological parameters, for the two surveys considered and different prior choices, are shown in Figures 11 − 12.

5.2.1 Constraints on CGM using using kSZ + tSZ

Strong degeneracies between the astrophysical parameters prevent us from getting any useful constraints on the CGM, using *only* cosmological priors i.e Prior-1 , when one uses either of the tSZ or the kSZ C_ℓ alone. However, once both the tSZ and the kSZ signals are added, the strong degeneracies are broken. This is seen clearly in the upper left

Table 2. Error on parameters for different surveys and Prior cases with fixed $\alpha_{\rm gas}$

Parameters	CV1000 , P1	CV1000 , P2	CV1000 , P3	SPT-like , P1	SPT-like , P2	SPT-like , P3
$\Delta\sigma_8$	0.0166	0.0163	0.0162	0.0270	0.0270	0.0270
$\Delta\Omega_M$	0.0163	0.0161	0.0161	0.020	0.020	0.020
Δn_s	0.0093	0.0093	0.0093	0.0094	0.0094	0.0094
Δh	0.0139	0.0139	0.0139	0.0140	0.0140	0.0140
$\Delta f_{\rm tratio}$	0.2329	0.2268	0.2266	18.7380	0.9986	0.9982
$\Delta f_{\rm Temp}$	0.0312	0.0311	0.0309	1.6547	1.4826	0.2465
$\Delta f_{\rm gas}$	0.0023	0.0023	0.0023	0.1119	0.0433	0.0366

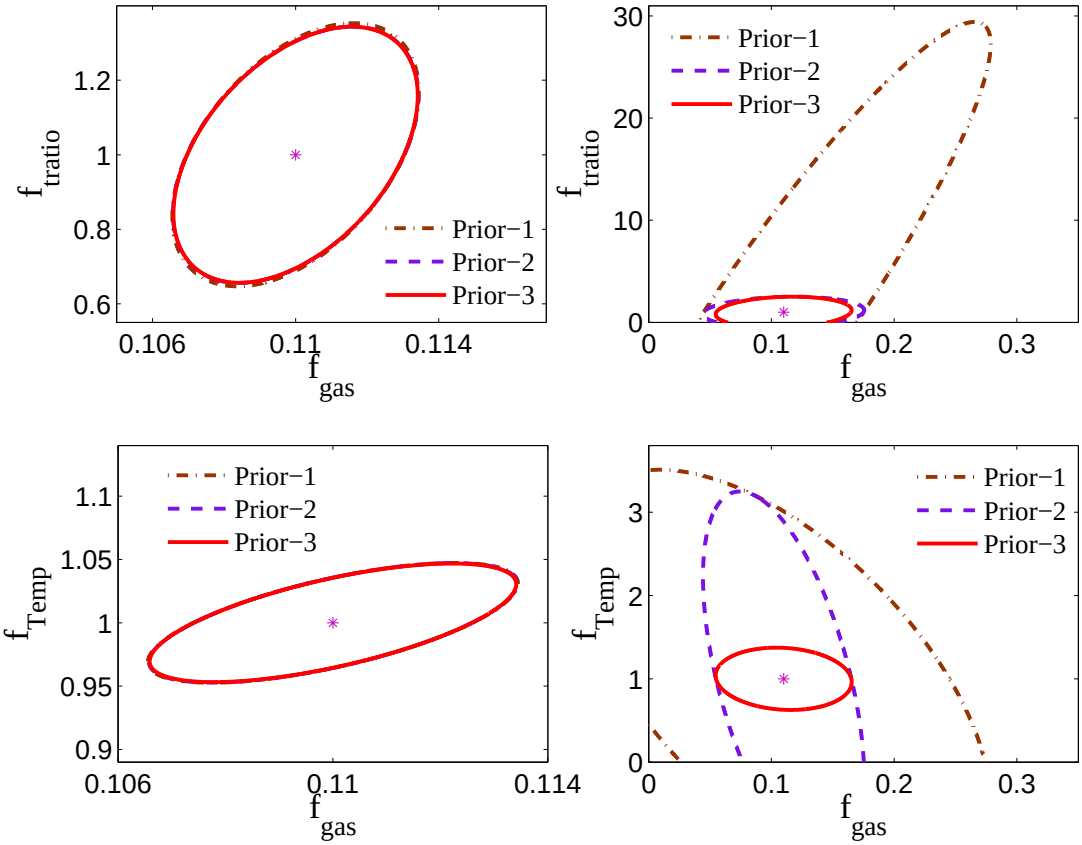

Figure 11. 1-σ contours for gas physics parameters $f_{\rm gas}, f_{\rm tratio}, f_{\rm Temp}$ when $\alpha_{\rm gas}$ is fixed. The left panel is for CV1000 survey and the right panel is for SPT-like survey. In all cases red solid line is Prior-3, purple dashed line is Prior-2 and brown dot-dashed line is Prior-1.

Table 3. Error on parameters for different surveys and Prior cases

Parameters	CV1000 , P1	CV1000 , P2	CV1000 , P3	SPT-like , P1	SPT-like , P2	SPT-like , P3
$\Delta\sigma_8$	0.0270	0.0263	0.0261	0.0270	0.0270	0.0270
$\Delta\Omega_M$	0.020	0.0187	0.0187	0.020	0.020	0.020
Δn_s	0.0094	0.0094	0.0094	0.0094	0.0094	0.0094
Δh	0.0140	0.0140	0.0140	0.0140	0.0140	0.0140
$\Delta f_{\rm tratio}$	0.5192	0.4608	0.4598	33.393	0.9995	0.9984
$\Delta f_{\rm Temp}$	0.0405	0.0396	0.0392	3.6606	1.9240	0.2479
$\Delta f_{\rm gas}$	0.0038	0.0035	0.0035	0.1687	0.1619	0.1404
$\Delta\alpha_{\rm gas}$	0.1052	0.0958	0.0954	4.0753	2.2890	1.7734

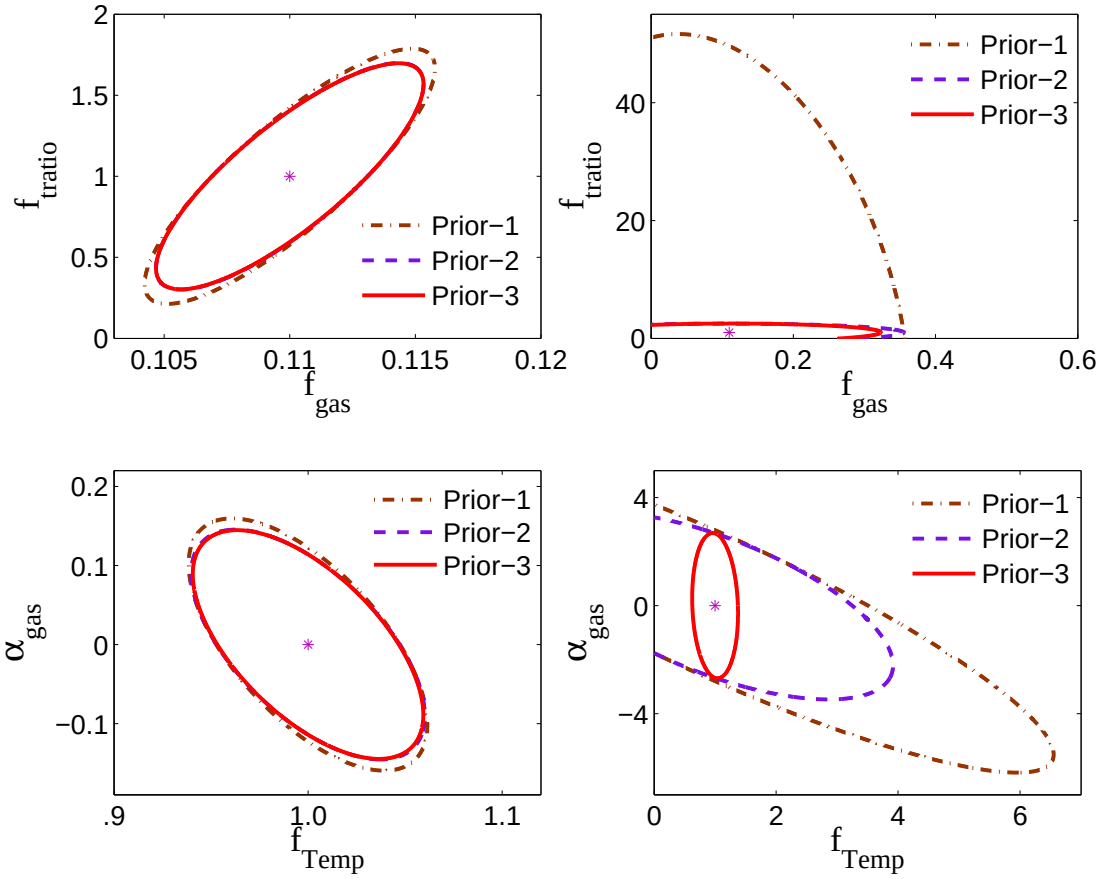

Figure 12. 1-σ contours for gas physics parameters $f_{\rm gas}, f_{\rm tratio}, f_{\rm Temp}, \alpha_{\rm gas}$. The left panel is for CV1000 survey and the right panel is for SPT-like survey. In all cases red solid line is Prior-3, purple dashed line is Prior-2 and brown dot-dashed line is Prior-1.

panel of Figure 9, which shows the joint constraint for the SPT-like survey. The fact that two cigar-like degeneracies, from two datasets, differing in their degeneracy directions eventually leads to very strong constraints in parameter space when taken together, is well known (see, for example, Khedekar, Majumdar & Das (2010)) and the same idea is at work here. Thus, although there is practically no constraint on $f_{\rm gas}$ from using tSZ or kSZ C_ℓ from CGM individually, adding them together results in a weak constraint of $\Delta f_{\rm gas} \approx 0.11$ which is the same as the fiducial value of $f_{\rm gas}$. One of reason for this weak constraint is the additional degeneracy of $f_{\rm gas}$ with α.

This degeneracy of $f_{\rm gas}$ with α is broken either (i) when one evokes no evolution in the Fisher analysis or (ii) when additional astrophysical priors are imposed. This is shown in the upper right and lower left panels of Figure 9. In both cases, the addition of astrophysical priors, for example Prior-3 , can already break the strong cigar like degeneracies leaving both kSZ and tSZ signal power to constrain $f_{\rm gas}$. The difference between these two panels is that α is not fixed (i.e we marginalise over unknown evolution) for the upper right panel leading to slightly weaker constraints (for tSZ+kSZ) than the lower left panel where α is held constant. The higher SNR of kSZ w.r.t tSZ (as seen in Figure 8) gives the kSZ C_ℓ a stronger constraining power on $f_{\rm gas}$ than tSZ and the addition of tSZ C_ℓ makes only modest improvement on the constraint on CGM achieved by using kSZ C_ℓ only.

The lower right panel of Figure 9 shows that constraints from the more futuristic cosmic variance limited survey CV1000 in the presence of Prior-3 but including an unknown gas fraction. In this case, due to its better sensitivity, tSZ is capable of constraining $f_{\rm gas}$ (compare green dashed ellipses in the two right panels, upper and lower) and finally comes up with stronger joint constraint than SPT-like (compare the red solid ellipse in lower left and and lower right). In the rest of this section, we focus mainly on constraints coming from kSZ+tSZ C_ℓ , keeping in mind that all the constraints will only be slightly degraded if only kSZ C_ℓ are used instead. Note that this is applicable as long as the astrophysical priors are added.

As evident above, one of the major uncertainties in our knowledge of the gas content of halos at all scales is our lack of understanding of any redshift evolution of the gas. In using large-scale structure data to constrain cosmology, for example, an unknown redshift evolution can seriously degrade cosmological constraints (as an example, see Majumdar & Mohr (2003)) and one needs to invoke novel ideas to improve constraints (Majumdar & Mohr

2004; Khedekar & Majumdar 2013). Whereas for galaxy clusters, in which case $f_{\rm gas}$ has been measured at higher redshift, and one finds evolution in gas content, no such evolution has been measured for galactic halos considered in this work. It is however possible that feedback processes in galaxies, and cosmological infall of matter may introduce an evolution of $f_{\rm gas}$ with redshift. In order to incorporate the impact of gas evolution on our constraints, we have considered the possibility that $f_{\rm gas}$ to scales with the expansion history $E(z)$ with a power-law index α, with the fiducial value of α set to 0.

The constraints on all the parameters used in the Fisher analysis for the cases where we assume the gas fraction to remain constant are given in Table 2. As mentioned before, in the absence of any astrophysical priors, there is no interesting constraints on $f_{\rm gas}$ (as well as $f_{\rm Temp}$ or $f_{\rm tratio}$) for SPT-like survey. However, for the CV1000 survey the amount of gas locked as CGM can be constrained very tightly to better than 2%; similarly, with cosmological priors only CV1000 can constraint departure from the virial temperature to 3.1% and $f_{\rm tratio}$ to $\sim 23\%$. The addition of astrophysical priors, either Prior-2 or Prior-3 does not improve the constraints for CV1000 any further, since the constraints with Prior-1 are much tighter than the priors imposed. However, astrophysical priors considerably improve the constraints for the SPT-like survey especially for $f_{\rm gas}$ *which is constrained to 39% when* Prior-2 *is used and is further constrained to better than 33% accuracy with* Prior-3 . This means that for both Prior-2 and Prior-3 , fg=0 can be excluded by at least 3σ with the SPT-like survey.

The corresponding constraint ellipses showing the 1σ allowed region between $f_{\rm gas}$ and either $f_{\rm Temp}$ or $f_{\rm tratio}$ are shown in Figure 11. The left panels show the degeneracy ellipses for CV1000 whereas the right panels show the same for SPT-like . Notice, from the upper panels, that $f_{\rm tratio}$ has a positive correlation with $f_{\rm gas}$. This can be understood by noting that any increase in $f_{\rm gas}$ increases C_ℓ whereas it can be offset by an increase $f_{\rm tratio}$ which pushes up the lowe limit of halo mass (see Figure 1) and hence decreases the number density of halos thus lowering the C_ℓ . The anti-correlation of $f_{\rm gas}$ with $f_{\rm Temp}$, seen in the lower right panel, is a consequence of the anti-correlation of n_e and T_v (in Equation 1) in the tSZ relation which modulates the overall degeneracy direction of tSZ+kSZ. Note that for the CV1000 survey, the 1σ ellipses are almost degenerate whereas priors shape the relative areas of the ellipses for the SPT-like survey.

A fixed non-evolving $f_{\rm gas}$, although desirable, is rather naive. Given our lack of understanding of the the energetics affecting the CGM over cosmic time scales, it is prudent to marginalise over any unknown evolution of $f_{\rm gas}$ parametrised, here, by α. The resultant constraints are given in Table 3. The presence over one extra unknown gas evolution parameter to marginalise over dilutes the constraints on $f_{\rm gas}$ for the both the surveys. For the CV1000 survey, the constraints are still strong and hovers around 3% for all the three prior choices. Moreover, $f_{\rm Temp}$ and $f_{\rm tratio}$ can be still be constrained to $\sim 4\%$ and $\sim 46\%$ by the futuristic survey. Without any external prior on α, all parameters poorly constrained by the SPT-like survey. With CV1000 survey, one can get a much stringent constraint on any possible evolution of the CGM with $\Delta\alpha \sim 0.1$

5.2.2 Constraints on Cosmology

The parameters of the standard cosmological model are already tightly constrained by *Planck*. These are the constrains that are used as Prior-1 in this paper. With the SNR possible in a SPT-like survey, it is not possible to tighten the cosmological constraints further irrespective of whether we know α or it is marginalized over. However, with the larger sensitivity of CV1000 survey, it is possible to further improve cosmological parameters, albeit with α fixed. A quick look at Table 2 shows that it is possible to shrink the 1σ error on σ_8 by almost a factor of 2 and that on Ω_M by $\sim 20\%$.

5.2.3 Constraints on the density profile of CGM

We have so far assumed the density profile of CGM to be uniform, which was argues on basis of current observations (Putman et al. 2012; Gatto et al. 2013). However, it is perhaps more realistic to assume that the density profile to decrease at large galacto-centric distances. One can ask if it would be possible to determine the pressure profile of the halo gas from SZ observations in the near future. In order to investigate this, we parameterise the density profile by γ_{gas} such that $\rho_{gas}(r) \propto (1 + (\frac{r}{R_s})^{\gamma_{gas}})^{-1}$, where R_s is the scale radius defined as $R_s \equiv R_{vir}/c(M, Z)$ and $c(M, Z)$ is the concentration parameter. This density profile gives uniform density at $r << R_s$ and $\rho_{gas}(r) \propto r^{-\gamma_{gas}}$ at $r >> R_s$. We include γ_{gas} in Fisher matrix analysis with fiducial value $\gamma_{gas} = 0$. For CV1000 survey with a fixed α_{gas} and Prior-3 , the constrain on density profile of CGM is $\gamma_{gas} < 1.5$ whereas the constrain degrades to $\gamma_{gas} < 3.15$ in the presence of an unknown redshift evolution of gas fraction. γ_{gas} poorly constrained by SPT-like survey.

6 SZ EFFECT FROM WARM CGM

The observations of Tumlinson et al. (2011) have shown the existence of OVI absorbing clouds, at $10^{5.5}$ K, with hydrogen column density $N_{\rm H} \sim 10^{19-20}$ cm^{-2}. The integrated pressure from this component in the galactic halo is estimated as $\langle p \rangle \sim N_{\rm H} kT$. This implies a thermal SZ $y-$ distortion of order $y_{OVI} \sim N_{\rm H} kT\sigma_T/(m_e c^2) \sim 3.6 \times 10^{-9}\, N_{\rm H,20}$, where $N_{\rm H} = 10^{20} N_{\rm H,20}$ cm^{-2}.

There is also a cooler component of CGM, at $\sim 10^4$ K, which is likely to be in pressure equilibrium with the warm CGM. The COS-Halos survey have shown that a substantial fraction of the CGM can be in the form of cold ($\sim 10^4$ K). Together with the warm OVI absorbing component, this phase can constitute more than half the missing baryons (Werk et al. 2014). Simulations of the interactions of galactic outflows with halo gas in Milky Way type galaxies also show that the interaction zone suffers from various instabilities, and forms clumps of gas at 10^4 K (Marinacci et al. (2010); Sharma et al. (2014)). These are possible candidates of clouds observed with NaI or MgII absorptions in galactic halos. Cross-correlating MgII absorbers with SDSS, WISE and GALEX surveys, Lan et al. (2014) have concluded that some of the cold MgII absorbers are likely associated with outflowing material. However, for similar column density of these clouds, the SZ signal would be less than that of the

warm components by $10^{-1.5}$ because of the temperature factor.

We can calculate the integrated y-distortion due to the CGM in intervening galaxies, by estimating the average number of galaxies in the appropriate mass range (10^{12-13} $M_\odot$) in a typical line of sight, using Monte-Carlo simulations. Dividing a randomly chosen line-of-sight, we divide it in redshift bins up to $z = 8$, and each redshift bin is then populated with halos using the Sheth-Tormen mass function, in the above mentioned mass range. We estimate the average number to be ~ 20 after averaging over 50 realisations. This implies an integrated y-parameter of order $7.5\times10^{-8}\, N_{\rm H,20}$. This can be detected with upcoming experiments such as Primordial Inflation Explorer (*PIXIE*) even with $N_{\rm H} = 10^{19}$ cm^{-2}, since it aims to detect spectral distortion down to $y \geqslant 2 \times 10^{-9}$ Kogut et al. (2011).

The kinetic SZ signal from the warm gas in galactic halos can be estimated from eqn 3, writing $v_{\rm local}$ as the local (line of sight) velocity dispersion. Recent studies indicate that CGM gas is likely turbulent, probably driven by the gas outflows (Evoli & Ferrara 2011). If we consider transonic turbulence for this gas, then $v_{\rm los}/c \sim \sqrt{kT/m_pc^2}$. Then we have,

$$\frac{\Delta T_{\rm kin}}{\Delta T_{\rm th}} \approx \frac{1}{2}\frac{m_e}{m_p}\sqrt{\frac{m_pc^2}{kT_e}} = \frac{m_e}{2m_p}\frac{c}{v_{\rm loc}}\,. \qquad (25)$$

For $v_{\rm loc} \sim 100$ km s^{-1} (corresponding to gas with temperature $\sim 10^6$ K), the kSZ signal from turbulent gas is, therefore, comparable to the tSZ signal.

7 CONCLUSIONS

We have calculated the SZ distortion from galactic halos containing warm and hot circumgalactic gas. For the hot halo gas, we have calculated the angular power spectrum of the distortion caused by halos in which the gas cooling time is longer than the halo destruction time-scale (galactic halos in the mass range of 5×10^{11}–$10^{13}h^{-1}$ $M_\odot$. The SZ distortion signal is shown to be significant at small angular scales ($\ell \sim 10^4$), and larger than the signal from galaxy clusters. The kinetic SZ signal is found to dominate over the thermal SZ signal for galactic halos, and also over the thermal SZ signal from galaxy clusters for $\ell > 10000$. We also show that the estimated Comptonization parameter $\tilde{Y}_{500}$ for most massive galaxies (halo mass $\geqslant 10^{12.5}$ $M_\odot$) is consistent with the marginal detection by *Planck*. The integrated Compton distortion from the warm CGM is estimated to be $y \sim 10^{-8}$, within the capabilities of future experiments.

Finally, we have investigated the detectability of the SZ signal for two surveys, one which is a simple extension of the SPT survey that we call SPT-like and a more futuristic cosmic variance limited survey termed CV1000 . We find that for the SPT-like survey, kSZ from CGM has a SNR of $\sim 2\sigma$ and at much higher SNR for the CV1000 survey. We do a Fisher analysis to assess the capability of these surveys to constrain the amount of CGM. Marginalizing over cosmological parameters, with *Planck* priors, and astrophysical parameters affecting the SZ C_ℓ from CGM, we find that in the absence of any redshift evolution of the gas fraction, the SPT-like survey can constrain $f_{\rm gas}$ to $\sim 33\%$, and the CV1000 survey, to $\sim 2\%$. Solving simultaneously for an unknown evolution of the gas fraction, the resultant constraints for CV1000 becomes 3% and it is poorly constrained by SPT-like survey. We also find that a survey like CV1000 can improve cosmological errors on σ_8 obtained by *Planck* by a factor of 2, if one has knowledge of the gas evolution. The Fisher analysis tells us that if indeed $\sim 10\%$ of the halo mass is in the circumgalactic medium, then this fraction can be measured with sufficient precision and can be included in the baryonic census of our Universe.

PS and BN would like to thank Jasjeet Singh Bagla and Suman Bhattacharya for helpful discussions. SM acknowledges the hospitality of Institute for Astronomy at ETH-Zurich where the project was completed during the the author's Sabbatical.

REFERENCES

Addison, G. E., Dunkley, J., Spergel, D. N. 2012, MNRAS, 427, 1741
Anderson, M. E., Bregman, J. N. 2010, ApJ, 714, 320
Anderson, M. E., Bregman, J. N. 2011, ApJ, 737, 22
Anderson, M. E., Bregman, J. N., Dai, X. 2013, ApJ, 762, 106
Anderson, M. E., Gaspari, M., White, S. D. M., Wang, M., Dai, W. 2014, arXiv:1409.6965v1
Benson, A. J., Bower, R. G., Frenk, C. S., White, S. D. M. 2000, 314, 557
Bhattacharya, S., Kosowsky, A. 2008, PhRvD, 3004B
Birnboim, Y., Dekel, A. 2003, MNRAS, 345, 349
Bogdán, Á, Gilfanov, M. 2011, MNRAS, 418, 1901
Bogdán, Á, Forman, W. R., Vogelsberger, M. et al.2013, ApJ, 772, 97
Bogdán, Á, Forman, W. R., Kraft, R. P., Jones, C. 2013, ApJ, 772, 98
Crain, R. A., McCarthy, I. G., Frenk, C. S., Theuns, T., & Schaye, J. 2010, MNRAS, 407, 1403
Dai, X., Anderson, M. E., Bregman, J. N., Miller, J. M. 2012, ApJ, 755, 107
Duffy, A. R., Battye, R. A., Davies, R. D., Moss, A., Wilkinson, P. N. 2008, MNRAS, 383, 150
Dutton, A. A., Conroy, C., vanden Bosch, F. C., Prada, F., More, S. 2010, MNRAS, 407, 2D
Efstathiou, G., Migliaccio, M. 2012, MNRAS, 423, 2492
Evoli, C., Ferrara, A. 2011, MNRAS, 413, 2721
Fang, T., Bullock, J., Boylan-Kolchin, M. 2013, ApJ, 762, 20
Forman, W., Jones, C., Tucker, W. 1985, ApJ, 293, 102
Fukugita, M., Hogan, C. J., Peebles, P. J. E., 1998, ApJ, 503, 518
Gatto, A., Fraternali, F., Read, J. I., et al. 2013, MNRAS, 433, 2749
Gradshteyn, I. S., Ryzhik, I. M. 1980, Tables of Integrals, Series and Products (New York: Academic Press)
Grcevich, J., Putman, M. E. 2009, ApJ, 696, 385
Hamana, T., Kayo, I., Yoshida, N., Suto, Y., Jing, Y. P. 2003, MNRAS, 343, 1312H
Jing, Y. P. 1999, ApJ, 515, L45
Khedekar, S., Majumdar, S., & Das, S., 2010, PRD, 82, 041301
Khedekar, S., & Majumdar, S., S., 2013, JCAP, 2, 30
Kogut, A, Fixsen, D. J., Chuss, D. T. et al.2011, JCAP, 7, 25
Komatsu, E., Kitayama, T. 1999, ApJ, 526L, 1K
Komatsu, E., Seljak, U. 2002, MNRAS, 336, 1256
Lacey, C., Cole, S. 1993, MNRAS, 262, 627
Lacey, C., Cole, S. 1994, MNRAS, 271, 676
Lan, T.-W., Ménard, B., Zhu, G. 2014, arXiv:1404.5301

Leauthaud, A., Tinker, J., Bundy, K., et al. 2012, ApJ, 744,159
Maccio A. V., Dutton A. A., Bosch F. C. van den, Moore B., Potter D., Stadel J., 2007, MNRAS, 378, 55
Majumdar, S., 2001, ApJ, 555, L7
Majumdar, S., & Mohr, J. J., 2003, ApJ, 585, 603
Majumdar, S., & Mohr, J. J., 2004, ApJ, 613, 41
Marinacci, F., Binney, J., Fraternali, F., Nipoti, C., Ciotti, L., Londrillo, P. 2010, MNRAS, 404, 1464
Maller, A. H., Bullock, J. S., 2004, MNRAS, 355, 694
Mitra, S., Kulkarni, G., Bagla, J. S., Yadav, J. K. 2011, BASI, 39, 563
Mo, H. J., Mao, S., White, S. D. M. 1998, MNRAS, 295, 319
Moster, B. P., Maccio, A. V., Somerville, R. S., Johansson, P. H., Naab, T. 2010, MNRAS, 403, 1009M
Planck Collaboration, 2013, A&A, 557, 52
Planck Collaboration, 2013, arXiv, 1303.507P
Putman, M. E., Peek, J. E. G., Joung, M. R. 2012, ARA&A, 50, 491
Rassmussen, J., Sommer-Larsen, J., Pedersen, K. et al.2009, ApJ, 697, 79
Silk, J. 1977, ApJ, 211, 638
Sharma, M., Nath, B. B., Chattopadhyay, I., Shchekinov, Y. 2014, MNRAS, 441, 431
Sharma, P., McCourt, M., Parrish, I. J., Quataert, E. 2012, MNRAS, 427, 1219
Sheth, R. K., Diaferio, A. 2001, MNRAS, 322, 901S
Sheth, R. K, Mo, H. J., Tormen, G. 2001, MNRAS, 323, 1S
Sutherland, R. S., Dopita, M. A. 1993, ApJ, 88, 253S
Tumlinson, J., Thom, C., Werk, J. et al.2011, Science, 334, 948
Walker, S. A., Bagchi, J., Fabian, A. C. 2014, arXiv:1411.1930v1
Werk, J. K., Prochaska, J. X., Tumlinson, J. et al.2014, arXiv:1403.0947
White, S. D. M., Rees, M. J. 1978, MNRAS, 183, 341
White, S. D. M., Frenk, C. S. 1991, ApJ, 379, 52